

Assessment of 3D aerodynamic effects on the behaviour of floating wind turbines

DManolas, V Riziotis, S Voutsinas

National Technical University of Athens, Laboratory of Aerodynamics, Greece

E-mail: manolasd@fluid.mech.ntua.gr

Abstract. Current state-of-art models for floating wind turbines are built by merging separate modules addressing the four basic aspects leading to a compound hydro-servo-aero-elastic time domain solver. While current state-of-the-art models differ in many aspects, they all use the blade element momentum (BEM) aerodynamic modelling. Due to its low cost, BEM is the standard choice for design purposes. However the use of BEM entails several semi-empirical corrections and add-ons that need reconsideration and recalibration when new features appear. For floating wind turbines, the effect of the floater motions is such a new feature. In the present paper, this aspect is investigated by comparing BEM based results against 3D free-wake simulations. Deterministic as well as stochastic simulations are presented in pure aerodynamic and full aeroelastic context. It is confirmed that asymmetric inflow originating from yaw misalignment and shear give significant differences reflected on mean values and amplitudes.

Key words: dynamics of floating wind turbine, free-wake aerodynamic model, vortex methods

1 Introduction

The behaviour of floating wind turbines is simulated by hydro-servo-aero-elastic time domain solvers combining appropriate modules for each of the four building blocks. While current state-of-the-art models differ in many aspects, they all use the blade element momentum (BEM) aerodynamic modelling [1]. BEM is a 1D flow theory suppressing a lot of the 3D characteristics of the flow around a wind turbine: radial dependence of the loading, non-axisymmetric inflow due to shear and/or yaw, wake induced effects. Several corrections are added in the BEM baseline theory in order to include the various effects not addressed by the formulation: the dynamic inflow, the 3D effects, the tip and root corrections. So far, verification of BEM aerodynamic modelling has been carried out almost exclusively for ground based wind turbines. Studies of this sort have concluded that BEM has difficulty in simulating asymmetric and time varying inflow, unless appropriate calibration is introduced that depends on the specific operational characteristics. Floating wind turbines constitute a relatively new concept that has not been analysed in depth partially due to lack of measurements. The new features of floating wind turbines refer mainly to the motions of the floater that eventually introduce additional dynamics to the relative inflow with respect to the rotor.

In the present work, simulations using BEM modelling are compared to those provided by the General Unsteady Vortex Particle (GENUVP) free-wake vortex aerodynamic modelling. These two aerodynamic modelling options are available in hydro-GAST [2] and therefore the two sets of simulations share the same hydro, servo and structural modelling. First, the BEM based version of hydro-GAST is verified for the spar-buoy floating 5MW reference wind turbine defined in the IEA



OC3 Annex on a code-to-code comparison basis. The comparison indicates that the overall modelling is consistent and comparable to the current state-of-the-art results. Based on that, a matrix of tests is defined and the signals obtained from BEM and GENUVP based simulations are compared in terms of mean value and amplitude. Anticipating that significant differences could occur in cases with strong asymmetric inflow, yaw misalignment, strong shear and wave direction are selected as main parameters in this study. Comparison with other free-wake or vortex type aerodynamic models has not been considered as to our knowledge there is no other vortex model for floating wind turbines.

2 Model overview

The behaviour of floating wind turbines is considered in the context of the dynamics of the whole construction subjected to external forcing and appropriate constraints/conditions. External forcing includes: the *aerodynamic loading* on the rotor blades due to the combined effect of wind inflow, rigid and elastic motions; the *hydrodynamic loading* on the floater and the *mooring reactions*; *inertial and gravitational loading*. Constraints are introduced mainly by the control system which in modern wind turbines corresponds to a variable pitch / variable speed controller. Also attachment conditions of the moorings at the sea bed will constrain the dynamics of the construction.

The dynamics of the system is modelled in the multi-body context. The wind turbine is divided in its components, which are either rigid (the floater) or flexible (blades, tower, drive train, mooring lines). The main flexible components are modelled as beams subjected to combined bending in two directions, tension and torsion. Currently, 2 options are available in hydro-GAST, a 2nd order Euler Bernoulli beam model and a linear Timoshenko beam model [5],[6],[7]. The latter is used in this work, following a “sub-body” approach [8]. Beams are divided into a number of inter-connected “sub-bodies”, each having its own coordinate system and with respect to which elastic deformations are defined. Dynamic and kinematic conditions are imposed at the connecting points. The preceding deformations are transferred as rigid body motions to the next “sub-body” which transfers back the corresponding loading. In this way, non-linear geometric effects due to large displacements are taken into account. The floater is modelled as a rigid body, connected to the wind turbine at the bottom of the tower. The position of the floater is defined by its 6 rigid body motions (3 translations and 3 rotations), which are constrained by the mooring lines. The mooring lines are considered as one-dimensional flexible components transmitting axial loads. Co-rotating non-linear truss elements are used [9]. Modelling of the interaction with the sea bed is carried out by introducing a series of vertical springs with appropriate (non-linear) characteristics that prevent the mooring line to get below the mud line. Lumped masses or buoys may be added.

Aerodynamic loading is defined in the context of aero-elasticity. As already mentioned, the focus of the present paper is on the 3D aerodynamic effects that are considered through free-wake modelling. In the present paper, the “thin-blade” version of GENUVP [10] is used. In this case, the vortex lattice modelling of the blades is applied while the evolution of the wake is approximated by means of freely moving vortex particles.

Using, Helmholtz’s decomposition, the velocity field $\vec{u}(\vec{x}; t)$ takes the form:

$$\vec{u}(\vec{x}; t) = \vec{U}_{\infty}(\vec{x}; t) + \nabla\varphi(\vec{x}; t) + \vec{u}_{\omega}(\vec{x}; t), \vec{x} \in D \quad (1)$$

$\vec{U}_{\infty}(\vec{x}; t)$ denotes the inflow velocity, $\nabla\varphi(\vec{x}; t)$ the disturbance velocity and $\vec{u}_{\omega}(\vec{x}; t)$ the wake induced velocity. In potential theory, wakes are introduced as vortex sheets, i.e. moving surfaces with potential and tangent velocity discontinuity $[[\varphi]]$, $[[\vec{u}]]$ respectively. It can be shown that such discontinuity surfaces can be identified to surface and line vorticity both in terms of the kinematics and the dynamics they generate in the flow. Actually the vortex lattice method originates from this idea. By assuming piecewise constant dipole distribution: $\mu = -[[\varphi]]$, surface vorticity $\vec{\gamma} = \nabla\mu \times \vec{\nu} \equiv 0$ ($\vec{\nu}$ being the normal unit vector) while line vorticity is defined as a closed vortex filament along the panel boundary with circulation equal to μ .

In the thin version of GENUVP, piecewise constant dipole distributions are defined on the blades and the “near-wake” which is the part of the wake that is generated within a time step. N_b , N_w denote the number of panels on the blades and the near wakes respectively so as: $N = N_b + N_w$. Vorticity emission is allowed along the trailing edge but also along the tip. Then, with $\vec{r} = \vec{x} - \vec{y}$ being the distance between the evaluation point \vec{x} and the control point \vec{y} , the potential and its gradient are:

$$\varphi(\vec{x}; t) = - \sum_{e=1}^N \mu^e(t) \int_{S^e} \frac{\vec{v}(\vec{y}; t) \cdot \vec{r}}{4\pi r^3} dS(\vec{y}) \Rightarrow \nabla \varphi(\vec{x}; t) = \sum_{e=1}^N \mu^e(t) \oint_{\partial S^e} \frac{d\vec{\ell}(\vec{y}) \times \vec{r}}{4\pi r^3} \quad (2)$$

In principle wake evolution can be followed using surface panelling. However strong deformations especially when the wake rolls-up, call for special attention and complicate the numerical scheme. A way to bypass these difficulties and also respect the fact that strong deformations in the wake lead to space vorticity distribution, is to approximate the vortex sheet as a collection of freely moving vortex particles. In the numerical model the transformation from surface to space vorticity is done when the “near-wake” is convected in preparing the next time step. The transformation is based on conservation of vorticity and its first moment [Figure 1] with $\vec{\Omega}$, \vec{Z} being the vorticity and the position vector of the vortex particle respectively:

$$\vec{\Omega} = \int \vec{\omega} dS, \vec{\Omega} \times \vec{Z} = \int \vec{\omega} \times \vec{x} dS \quad (3)$$

The induced velocity at the evaluation point \vec{x} from the wake (vortex particles) is:

$$\vec{u}_\omega(\vec{x}, t) = \sum_{j \in J(t)} \frac{\vec{\Omega}_j(t) \times (\vec{x} - \vec{Z}_j(t))}{4\pi |\vec{x} - \vec{Z}_j(t)|^3} f(|\vec{x} - \vec{Z}_j(t)|/\varepsilon) \quad (4)$$

$f(r/\varepsilon) = 1 - \exp(-(r/\varepsilon)^3)$ is the regularizing function and ε the cut-off length, chosen so that core overlapping is ensured.

The unknown dipole intensities are determined by the flow conditions on the blade surfaces and along the emission lines. On the blade surface, μ^e is determined by the “no-penetration” boundary condition. Note that this condition must include the rigid body motions and the deformation velocities, while the deformed geometry is also explicitly needed. In this way a fully non-linear aeroelastic coupling is introduced. As regards the wake, μ^e on the “near-wake” is determined by the Kutta condition specifying zero vorticity along the emission line which means that at emission the dipole intensity of the wake panel is equal to the intensity of the adjacent panel of the blade. Then for the rest of the wake, evolution is carried out by convecting and deforming the vortex blobs:

$$\frac{d\vec{Z}_j(t)}{dt} = \vec{u}(\vec{Z}_j; t), \quad \frac{d\vec{\Omega}_j(t)}{dt} = (\vec{\Omega}_j(t) \cdot \nabla) \vec{u}(\vec{Z}_j; t) \quad (5)$$

The model as such is 3D, but potential. Therefore correction of the aerodynamic loads is needed. In GENUVP, this is done using the generalised ONERA model with the following modifications: the attached part of the lift circulation is obtained directly from the flow solver; the effective angle of attack is defined by the sectional circulation; the effective inflow velocity is taken as the mean over the panels of the section. These amendments refer to the flow characteristics in the chord scale and not the diameter scale in which the 3D aerodynamic model is free of simplifying assumptions and therefore represent reality more accurately.

The hydrodynamic forcing on the floater includes: hydrostatic forces; the wave induced forces taking into account the presence of the body (diffraction); radiation forces due to floater’s motion; non-linear viscous drag. Currently the first order hydrodynamic theory is used [11]. In brief, based on the superposition principle, applicable to linear problems, the diffraction and radiation problem is first solved in the frequency domain and then transformed into the time domain. The impulse response

function method [12] is applied for the radiation forces, while for the diffraction problem the synthesis of the effect of a wave pattern of given spectrum is based on random phase-lagged simple harmonic responses. Optionally, the viscous drag force from the Morison equation is added, providing additional hydrodynamic damping. For the mooring lines, the hydrodynamic loading is taken into account using the relative form of the Morison's equation.

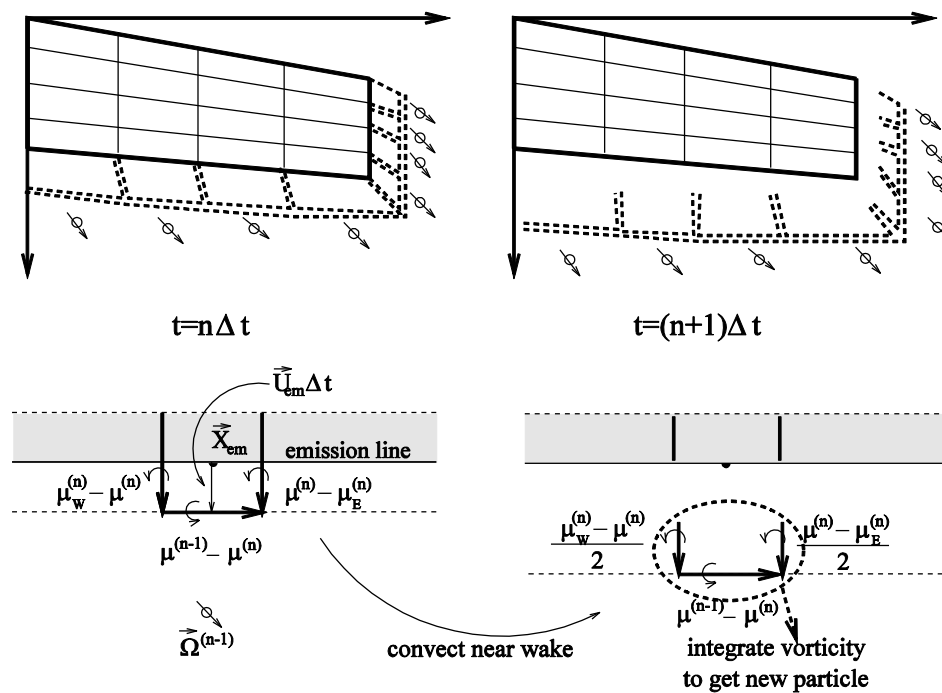


Figure 1: The hybrid scheme of the wake

3 Results and discussion

All simulations concern the NREL 5MW OC3 floating wind turbine [1], [3], [4] which is a variable pitch variable speed machine. The OC3 controller as defined in [3], [4] is used, with the addition of a drive train damper at 1.7 Hz. The results are divided into four groups. The first concerns the load cases defined in OC3 [Table 1]. The full model is considered (i.e. with the controller and all the degrees of freedom enabled). In order to have comparable results with those reported in [1], this set is using the BEM aerodynamic model of hydro-GAST. The intension of this exercise is to evaluate the simulations hydro-GAST is producing in comparison to other existing tools and by that to verify the overall modeling setup. The second set of results focuses on cases in which 3D aerodynamic effects such like wind shear and yaw misalignment, are known to have an important role [Table 2]. In this set the controller has been switched off, in order to confine attention on the aerodynamic effects. Next, in the third set of results, the controller is enabled, and selected cases from the second set are recalculated. Finally in the fourth set, BEM and GENUVP based stochastic simulations for the OC3 dlc5.2 and 5.3 cases are compared in terms of statistics and damage equivalent loads [Table 1].

3.1 The OC3 cases

Comparisons between hydro-GAST and OC3 results from the load case 5.1 are made in Figure 2 for selected signals. The hydro-GAST results are close to the majority of the results both in terms of mean values and amplitudes. Similar agreement is found in all signals. Therefore it is confirmed that the overall modelling of the spar buoy floating wind turbine in hydro-GAST is consistent.

Table 1: OC3 Phase IV load cases

dlc	Wind Condition	Wave Condition
5.1	Steady, Uniform, No Shear: $V_{hub} = 8\text{m/s}$	NSS: Regular Airy, $H = 6\text{m}$, $T_p = 10\text{s}$
5.2	NTM: $V_{hub} = 11.4\text{m/s}$, $I_{ref} = 0.14$ (B), turbulence model = Mann	NSS: Irregular Airy, $H_s = 6\text{m}$, $T_p = 10\text{s}$
5.3	NTM: $V_{hub} = 18\text{m/s}$, $I_{ref} = 0.14$ (B), turbulence model = Mann	NSS: Irregular Airy, $H_s = 6\text{m}$, $T_p = 10\text{s}$

Table 2: Deterministic cases

	Uniform	Wind shear exp 0.2	yaw +15	yaw -15
8m/s	<u>0°/30°</u> wave direction	<u>0°/30°</u> wave direction	<u>0°/30°</u> wave direction	0°/30° wave direction
11.4m/s	<u>0°/30°</u> wave direction	<u>0°/30°</u> wave direction	<u>0°/30°</u> wave direction	0°/30° wave direction

* the underlined cases have been considered in the 3rd set of results (controller ON)
+ Wave characteristics: Airy wave with $T=10\text{sec}$ and height=8m.

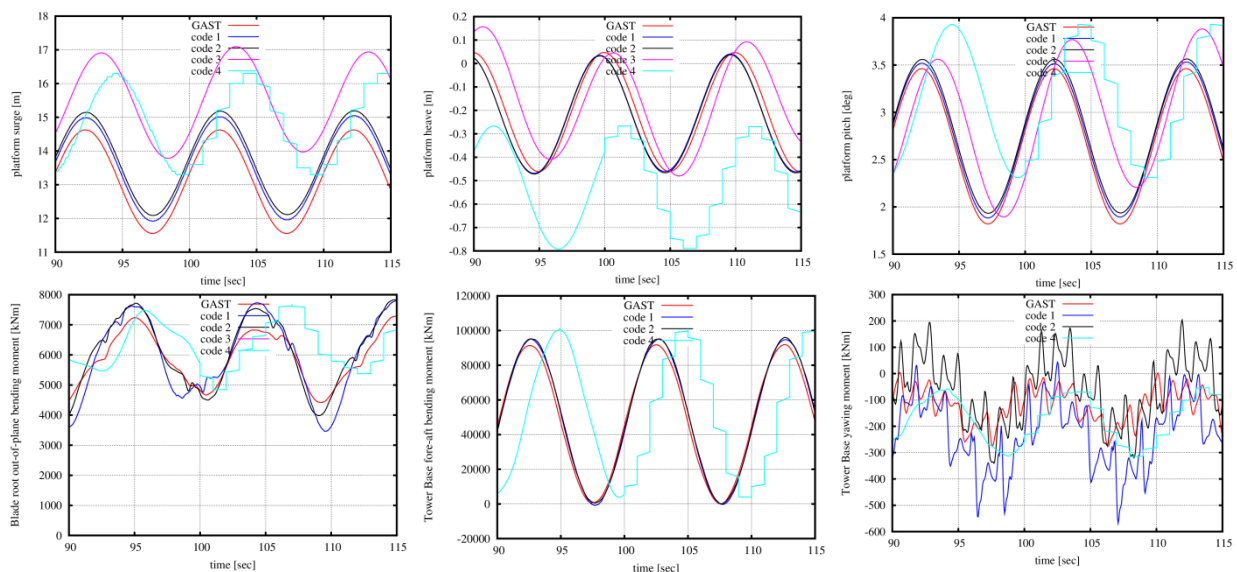


Figure 2: Comparisons between BEM based hydro-GAST predictions and four state-of-art codes for the 5.1 load case of OC3. Upper row: surge, heave and pitch of the floater; Lower row: blade out-of-plane bending moment, tower bottom fore-aft moment and yawing moment.

3.2 Deterministic load cases without controller

As already mentioned, in the 2nd set of simulations the controller is switched off. Two different wind speeds are considered at 8m/s and 11.4m/s with constant rotational speeds 9rpm and 12rpm respectively. The pitch angle is set to 0°. Results are presented in terms of mean value and amplitude in **Tables 3&4**. “B” stands for BEM and “G” for GENUVP. “e” is the absolute relative difference with respect to GENUVP results.

In general, BEM predicts higher aerodynamic thrust, which in turn increases the mean values of the floater’s surge and pitch motions. Increased surge motion (at positive x) reduces the length of the two moorings sitting on the sea bed, so the moorings actual weight is increased, leading to reduced mean value of the heave motion. The difference of the mean values of the floater motions is ~10%, while the

amplitudes of the motions are almost the same for all the floater motions except yaw which in any case attains small absolute values. The specific wind shear and yaw misalignment have small effect on the floater motions.

Table 3: Deterministic results for 0° wave angle – no controller

		Uniform 8m/s		Uniform 11.4m/s		Shear 8m/s		Shear 11.4m/s		Yaw+15° 8m/s		Yaw+15° 11.4m/s		Yaw-15° 8m/s		Yaw-15° 11.4m/s	
		mean	amp	mean	amp	mean	amp	mean	amp	mean	amp	mean	amp	mean	amp	mean	Amp
Floater surge [m]	B	12.6	4.5	25.2	4.3	12.9	4.3	25.2	4.0	12.3	4.3	24.3	4.1	12.4	4.2	24.3	4.1
	G	11.2	4.5	22.8	4.2	11.7	4.3	22.8	4.0	11.4	4.2	22.4	4.0	11.5	4.1	22.4	4.0
	e	0.13	0.01	0.11	0.03	0.10	0.01	0.11	0.01	0.08	0.03	0.08	0.01	0.08	0.02	0.09	0.03
Floater heave [m]	B	-0.198	0.759	-0.593	0.822	-0.201	0.723	-0.591	0.773	-0.176	0.700	-0.538	0.693	-0.198	0.704	-0.578	0.691
	G	-0.169	0.754	-0.497	0.838	-0.172	0.725	-0.521	0.799	-0.165	0.690	-0.468	0.707	-0.175	0.688	-0.496	0.693
	e	0.17	0.01	0.19	0.02	0.17	0.00	0.14	0.03	0.07	0.01	0.15	0.02	0.14	0.02	0.17	0.00
Floater pitch [deg]	B	2.58	2.16	5.04	2.11	2.58	2.15	5.03	2.11	2.46	2.14	4.81	2.10	2.46	2.16	4.81	2.11
	G	2.33	2.14	4.55	2.08	2.43	2.13	4.55	2.08	2.27	2.12	4.42	2.07	2.29	2.12	4.44	2.07
	e	0.10	0.01	0.11	0.01	0.06	0.01	0.11	0.01	0.08	0.01	0.09	0.02	0.07	0.02	0.08	0.02
Floater yaw [deg]	B	-0.069	0.837	-0.132	0.809	0.057	0.927	0.158	1.026	-0.462	0.554	-0.778	0.398	0.331	1.253	0.497	1.217
	G	-0.107	0.995	-0.242	0.868	0.014	1.245	-0.052	1.292	-0.229	1.167	-0.562	1.169	0.018	0.850	0.066	0.547
	e	0.35	0.16	0.45	0.07	3.19	0.26	4.01	0.21	1.02	0.53	0.38	0.66	17.71	0.47	6.49	1.22
Flap-wise moment [kNm]	B	5738	4032	10440	4983	5662	3971	10286	4973	5470	3736	9931	4845	5489	4758	10015	6281
	G	5474	4865	9873	5498	5410	4681	9754	5298	5353	4559	9631	5641	5355	5187	9634	6070
	e	0.05	0.17	0.06	0.09	0.05	0.15	0.05	0.06	0.02	0.18	0.03	0.14	0.02	0.08	0.04	0.03
Side-to- side moment [kNm]	B	2836	3725	5701	4822	3398	3583	6823	4354	2496	3792	5258	4382	2698	3903	5145	4481
	G	2695	3992	5276	4383	3246	3942	6162	4266	2775	3931	5628	3913	2436	3968	4210	4142
	e	0.05	0.07	0.08	0.10	0.05	0.09	0.11	0.02	0.10	0.04	0.07	0.12	0.11	0.02	0.22	0.08
Fore-aft moment [kNm]	B	44869	123106	88921	116679	45187	123564	89294	116989	42565	123835	84693	118391	42633	123535	84608	114826
	G	40435	124515	79808	119523	45500	125101	80580	120005	39070	124564	77188	120030	39716	124480	77915	118622
	e	0.11	0.01	0.11	0.02	0.01	0.01	0.11	0.03	0.09	0.01	0.10	0.01	0.07	0.01	0.09	0.03
Yawing moment [kNm]	B	-137	498	-456	658	104	656	281	678	-890	469	-1509	702	632	930	938	805
	G	-205	649	-640	731	-44	979	-120	1042	-441	855	-1093	720	29	569	112	512
	e	0.34	0.23	0.29	0.10	3.37	0.33	3.34	0.35	1.02	0.45	0.38	0.03	20.46	0.64	7.41	0.57
Torque [kNm]	B	2032	2729	4185	3910	1983	2771	4074	3945	1852	2711	3850	3810	1852	2608	3834	3768
	G	2015	3224	4100	4359	1913	3326	3999	4402	1910	3217	3880	4257	1919	3194	3880	4301
	e	0.01	0.15	0.02	0.10	0.04	0.17	0.02	0.10	0.03	0.16	0.01	0.11	0.04	0.18	0.01	0.12

In terms of loads, BEM predicts higher mean loads compared to GENUVP with differences that range from 1% to more than 100%. Differences higher than 10% concern the yawing moment. BEM predicts 2%-5% higher mean values for the flap-wise bending moment on the blade, while GENUVP predicts about 10% higher amplitudes. Amplitude differences are higher at 8m/s, while shear and yaw reduce them in comparison to the uniform wind inflow case. For the tower bottom bending moments, a 10% difference in the mean value is observed, while the amplitudes are the same when the motion is driven from the wave (i.e. the fore-aft direction and the side-to-side direction when the wave angle is 30°). About 10% differences are observed for the amplitude of the side-to-side bending moment for

the zero wave angle cases. The two models give similar mean values of the shaft torque while GENUVP predicts 10%-18% higher amplitudes. The edge-wise bending moment and the pitching moment at the root of the blade, are almost the same, and are not showed in the tables. Taking into account the formulation of the two models, these differences are associated to the different wake modelling.

Table 4: Deterministic results for 30° wave angle – no controller

		Uniform 8m/s		Uniform 11.4m/s		Shear 8m/s		Shear 11.4m/s		Yaw+15° 8m/s		Yaw+15° 11.4m/s		Yaw-15° 8m/s		Yaw-15° 11.4m/s	
		mean	amp	mean	amp	mean	amp	mean	amp	mean	amp	mean	amp	mean	amp	mean	amp
Floater surge [m]	B	12.6	3.8	25.3	3.9	12.8	3.9	25.1	3.4	12.3	3.7	24.3	3.5	12.4	3.6	24.4	3.6
	G	11.3	3.8	22.9	3.7	11.7	3.9	22.8	3.4	11.5	3.9	22.5	3.4	11.7	3.7	22.5	3.5
	e	0.11	0.02	0.10	0.05	0.09	0.01	0.10	0.00	0.08	0.03	0.08	0.01	0.06	0.03	0.08	0.04
Floater heave [m]	B	-0.204	0.723	-0.594	0.823	-0.201	0.697	-0.595	0.703	-0.178	0.695	-0.537	0.718	-0.202	0.697	-0.582	0.698
	G	-0.184	0.707	-0.498	0.821	-0.184	0.733	-0.530	0.697	-0.174	0.710	-0.474	0.714	-0.178	0.709	-0.503	0.694
	e	0.11	0.02	0.19	0.00	0.09	0.05	0.12	0.01	0.02	0.02	0.13	0.01	0.14	0.02	0.16	0.01
Floater pitch [deg]	B	2.60	1.90	5.06	1.86	2.59	1.88	5.05	1.83	2.47	1.89	4.82	1.85	2.46	1.87	4.82	1.84
	G	2.37	1.88	4.59	1.83	2.37	1.86	4.57	1.81	2.30	1.86	4.45	1.82	2.31	1.86	4.45	1.82
	e	0.10	0.01	0.10	0.01	0.09	0.01	0.10	0.01	0.07	0.02	0.08	0.02	0.07	0.01	0.08	0.01
Floater yaw [deg]	B	-0.046	2.380	-0.086	3.916	0.065	2.377	0.164	3.815	-0.452	1.734	-0.748	3.013	0.330	2.509	0.518	3.846
	G	-0.087	2.168	-0.200	3.117	-0.025	2.235	-0.050	3.096	-0.221	2.070	-0.546	2.909	0.013	1.835	0.070	2.618
	e	0.48	0.10	0.57	0.26	3.62	0.06	4.32	0.23	1.05	0.16	0.37	0.04	25.21	0.37	6.43	0.47
Flap- wise moment [kNm]	B	5777	4063	10475	5474	5683	3979	10312	5345	5505	3424	9953	5063	5506	4757	10035	6497
	G	5532	4670	9942	5543	5461	4492	9803	5439	5412	4388	9713	5241	5392	4950	9673	6015
	e	0.04	0.13	0.05	0.01	0.04	0.11	0.05	0.02	0.02	0.22	0.02	0.03	0.02	0.04	0.04	0.08
Side-to- side moment [kNm]	B	2915	66011	6416	61920	3520	64399	6167	62732	2644	65112	6075	62899	2798	62998	5705	58740
	G	2634	66587	5580	62459	3255	64736	5674	62194	2735	64198	5881	62319	2418	64363	4546	60793
	e	0.11	0.01	0.15	0.01	0.08	0.01	0.09	0.01	0.03	0.01	0.03	0.01	0.16	0.02	0.25	0.03
Fore-aft moment [kNm]	B	45506	107182	89764	102633	45756	107381	89586	103033	43074	107208	84765	105078	43097	108017	85405	101808
	G	41287	108071	80862	104934	41841	108559	81029	105207	40024	108216	77932	105225	40306	108005	78613	105314
	e	0.10	0.01	0.11	0.02	0.09	0.01	0.11	0.02	0.08	0.01	0.09	0.00	0.07	0.00	0.09	0.03
Yawing moment [kNm]	B	-129	612	-275	1921	121	607	105	4124	-874	717	-1633	3699	643	552	937	1586
	G	-197	681	-475	1931	-48	721	-278	3570	-425	533	-1230	3474	42	572	112	2018
	e	0.35	0.10	0.42	0.01	3.55	0.16	1.38	0.16	1.06	0.35	0.33	0.06	14.16	0.03	7.38	0.21
Torque [kNm]	B	2020	2506	4175	3518	1966	2523	4084	3500	1838	2480	3836	3566	1831	2402	3830	3407
	G	2005	2893	4107	3893	1966	2963	3985	3889	1906	2846	3885	3694	1895	2845	3874	3894
	e	0.01	0.13	0.02	0.10	0.00	0.15	0.02	0.10	0.04	0.13	0.01	0.03	0.03	0.16	0.01	0.13

The 30° wave direction mainly alters the side loads and floater motions. Because the wave drives the fore-aft and the side-to-side motions of the floater, the effect of modelling differences is reduced. The differences in the yaw moment and motion are eliminated, because of the couplings between the motions. The yawing moment is still the load with the maximum divergence, especially for the shear and yaw cases in which the wake induced effects are not as pronounced in the BEM results. For all cases except the yaw+15 at 8m/s, BEM predicts slightly higher mean values for the side-to-side tower

moment, while the amplitudes are identical. The wave misalignment reduces the differences in the floater yaw motion, but not in the surge, the heave and the pitch which remain the same.

Table 5: Deterministic results for 0° wave angle – controller enabled

		Uniform 8m/s		Uniform 11.4m/s		Shear 8m/s		Shear 11.4m/s		Yaw+15° 8m/s		Yaw+15° 11.4m/s	
		mean	amp	mean	amp	mean	amp	mean	amp	mean	amp	mean	amp
Floater surge [m]	B	13.3	4.1	21.4	3.7	12.5	4.3	21.9	3.8	12.5	4.2	23.1	3.8
	G	12.1	4.1	19.9	4.0	11.2	4.3	20.3	4.0	11.7	4.2	20.9	4.1
	e	0.10	0.01	0.07	0.06	0.12	0.01	0.08	0.04	0.07	0.01	0.10	0.08
Floater heave [m]	B	-0.193	0.784	-0.437	0.817	-0.177	0.707	-0.457	0.826	-0.163	0.900	-0.482	0.887
	G	-0.165	0.788	-0.393	0.813	-0.163	0.709	-0.432	0.812	-0.153	0.887	-0.406	0.871
	e	0.17	0.00	0.11	0.01	0.09	0.00	0.06	0.02	0.06	0.01	0.19	0.02
Floater pitch [deg]	B	2.67	2.18	4.27	1.92	2.60	2.30	4.40	1.89	2.47	2.19	4.56	1.98
	G	2.43	2.16	4.02	1.93	2.35	2.27	4.14	1.96	2.31	2.18	4.14	2.01
	e	0.10	0.01	0.06	0.01	0.10	0.01	0.06	0.03	0.07	0.01	0.10	0.01
Floater yaw [deg]	B	-0.073	0.417	-0.218	0.944	0.059	0.560	0.154	0.825	-0.478	0.136	-0.701	0.558
	G	-0.105	0.652	-0.253	1.061	-0.035	0.875	-0.018	0.846	-0.229	0.878	-0.525	1.092
	e	0.31	0.36	0.14	0.11	2.66	0.36	9.40	0.03	1.09	0.85	0.33	0.49
Flap-wise moment [kNm]	B	5933	4049	8937	6301	5780	4372	9073	7113	5527	3925	9512	6172
	G	5654	4886	8843	6526	5532	5114	8974	7080	5427	4827	9167	6315
	e	0.05	0.17	0.01	0.03	0.04	0.15	0.01	0.00	0.02	0.19	0.04	0.02
Side-to- side moment [kNm]	B	2745	721	5163	5050	3167	1463	6436	8273	2416	2172	5269	7358
	G	2647	753	4733	9823	3047	1844	5667	5761	2712	1533	5346	3467
	e	0.04	0.04	0.09	0.49	0.04	0.21	0.14	0.44	0.11	0.42	0.01	1.12
Fore-aft moment [kNm]	B	46263	120818	74919	131268	46016	127020	78010	129486	42843	122446	80306	122084
	G	41954	122123	70210	128276	41608	127472	73013	126208	39725	122805	72226	125615
	e	0.10	0.01	0.07	0.02	0.11	0.00	0.07	0.03	0.08	0.00	0.11	0.03
Yawing moment [kNm]	B	-143	232	-435	558	66	541	275	722	-919	401	-1367	656
	G	-206	397	-492	719	-115	889	-41	758	-437	644	-1024	734
	e	0.31	0.41	0.12	0.22	1.57	0.39	7.78	0.05	1.10	0.38	0.33	0.11
Torque [kNm]	B	2016	450	3932	1537	1977	513	3886	1504	1862	541	3793	1514
	G	2004	561	3813	1635	1961	634	3779	1617	1902	622	3733	1535
	e	0.01	0.20	0.03	0.06	0.01	0.19	0.03	0.07	0.02	0.13	0.02	0.01
Shaft Omega [rpm]	B	9.31	0.99	12.10	1.72	9.25	1.04	12.10	1.64	9.05	0.93	12.10	1.36
	G	9.31	1.16	12.10	1.75	9.24	1.22	12.10	1.68	9.13	1.13	12.06	1.59
	e	0.00	0.15	0.00	0.02	0.00	0.15	0.00	0.03	0.01	0.18	0.00	0.14
Blade Pitch [deg]	B	0.00	0.00	2.28	3.59	0.00	0.00	1.92	3.49	0.00	0.00	0.89	2.33
	G	0.00	0.00	1.56	3.30	0.00	0.00	1.25	2.95	0.00	0.00	0.83	2.35
	e	0.00	0.00	0.46	0.09	0.00	0.00	0.53	0.18	0.00	0.00	0.07	0.01

3.3 Deterministic load cases with controller

The 3rd set of results corresponds to selected cases from **Table 2** with the controller enabled. The results are given in **Table 5**, for 0 wave direction. At the below rated wind speed, the controller

activates the rotational speed variation. GENUVP predicts higher amplitudes for the rotational speed, while the mean values are the same. The difference in amplitude is connected to the controller which was calibrated on the basis of BEM simulations. A different tuning could eventually reduce these amplitudes. The differences between BEM and GENUVP results agree with the previous “no controller” cases.

At the rated wind speed of 11.4m/s, due to pitch control, the rotational speed reaches its nominal value. Now high differences are noted in blade pitch which suggests incompatibility with the controller tuning. The differences in the flap-wise bending moment and shaft torque are eliminated, while the differences in the tower yawing and side-to-side moments persist.

3.4 Stochastic simulations

Results from the two stochastic load cases of the OC3 are compared in **Table 6** in terms of 1Hz damage equivalent loads (DEL) and statistics. The DELs are calculated at the blade root ($m=12$), at the tower bottom ($m=4$) and at the main bearing ($m=8$). Although in the previous test cases the action of the controller seemed to eliminate the differences between the two models, BEM overestimates the flap-wise bending moment by 15% compared to the GENUVP results. The tower bottom fore-aft moment is overestimated for only 2%. The present indicative results suggest that BEM predictions for the specific load cases lay on the safe side.

Table 6: Equivalent loads and Statistics

dlc	Loads [kNm]	DEL			Mean Value			Standard Deviation		
		BEM	GEN	e	BEM	GEN	e	BEM	GEN	e
dlc5.2	Edgewise moment	7063	6969	-0.01	918	1005	0.09	2528	2516	0.00
	Flapwise moment	8473	7481	-0.13	8632	8725	0.01	1918	1739	-0.10
	Pitching moment	131	134	0.02	-4	-5	0.19	35	36	0.03
	Side-to-side moment	7794	8017	0.03	6318	6184	-0.02	3098	3235	0.04
	Fore-aft moment	63765	62412	-0.02	74478	71323	-0.04	26602	25902	-0.03
	Yawing moment	4124	4176	0.01	-322	-615	0.48	1707	1677	-0.02
	Shaft Torque	1201	1172	-0.02	3686	3716	0.01	562	527	-0.07
dlc5.3	Edgewise moment	7519	7337	-0.02	240	251	0.04	2485	2515	0.01
	Flapwise moment	11646	9938	-0.17	4735	5211	0.09	2657	2336	-0.14
	Pitching moment	148	147	-0.01	-32	-32	-0.02	34	33	-0.01
	Side-to-side moment	14694	14015	-0.05	8917	8211	-0.09	5097	4642	-0.10
	Fore-aft moment	74981	73436	-0.02	45977	43527	-0.06	28462	28143	-0.01
	Yawing moment	6105	5641	-0.08	-461	-434	-0.06	2543	2176	-0.17
	Shaft Torque	1096	1017	-0.08	4180	4180	0.00	242	228	-0.06

4 Conclusions

The BEM and GENUVP (free-wake) aerodynamic models in hydro-GAST, are used in order to analyze the 3D aerodynamic effects on spar-buoy floating wind turbines. First the BEM version of hydro-GAST is compared to other state-of-art models of similar theoretical background for the OC3 load cases defined for the spar-buoy floating concept. Similar results have been obtained indicating that the overall modeling context of hydro-GAST is consistent and valid under the following specific assumptions: BEM aerodynamic modeling and linear hydrodynamics.

Next simulations using the BEM and GENUVP versions of hydro-GAST are compared for various deterministic and stochastic loads. Out of these comparisons the following conclusions can be drawn:

1. Application of the BEM aerodynamic modeling to a spar-buoy floating WT is found to provide higher loads and therefore is on the safe side. This is important especially since the difference in cost between BEM and GENUVP is substantial. When turbulent wind inflow is considered, the difference in run time is in the order of 50.
2. The averaged difference between the two models is ~15% for the blade loading and ~5% for the tower loading. Disregarding the various uncertainties in modeling, such a difference will have an impact on the cost and therefore should be considered in more detail.
3. As expected the highest differences appear in asymmetric inflow conditions. Assuming that free-wake modeling is of higher fidelity, then one possible use of more sophisticated models is to provide the basis for better calibrating the modeling of yaw and shear in BEM. Note that a yaw misalignment of 15° corresponds to the limit beyond which yaw correction is activated. Higher yaw angles should be considered in view of assessing also extreme / fault load cases.
4. In the present study, BEM and GENUVP aerodynamic models are compared considering normal sea state, within the context of linear hydrodynamic theory, applied to the spar-buoy floater case. Other floating concepts as well as different sea states should be checked in future studies.
5. Of particular importance is the role of the controller. Results indicate that the controller can reduce the differences, indicating that a better tuned controller or an adaptive controller can substantially reduce loading and limit the level of uncertainties.

Clearly the above conclusions are subjected to the limited number of load cases considered. A full load spectrum and an estimation of extreme loads is needed in order to firmly conclude that BEM remains on the safe side and estimate the relevant safety margin in case of floating wind turbines.

References

- [1] Jonkman J, Musial W, 2010, "Final Report, Subtask 2", "The Offshore Code Comparison Collaboration (OC3)", IEA Wind Task 23.
- [2] hydro-GAST technical report, http://www.aerolab.ntua.gr/hydroGAST_report.pdf
- [3] Jonkman J, Butterfield S, Musial M, Scott, G, 2009, "Definition of a 5-MW Reference Wind Turbine for Offshore System Development", Technical Report, NREL/TP-500-38060, USA.
- [4] Jonkman J, 2010, "Definition of the Floating System for Phase IV of OC3", Technical Report NREL/TP-500-47535, USA.
- [5] Riziotis VA, Voutsinas SG, 1997, "GAST: A general aerodynamic and structural prediction tool for wind turbines", EWEC'97 Dublin Ireland.
- [6] Riziotis V.A., Voutsinas S.G., Manolas D.I., Politis E.S. and Chaviaropoulos P.K., "Aeroelastic Analysis of Pre-Curved Rotor Blades," EWEC 2010.
- [7] Riziotis VA et al, 2004, "Aeroelastic Stability of Wind Turbines: the problem, the methods, the issues", Wind Energy, V. 7, p 373-392
- [8] Riziotis VA, Voutsinas SG, Politis ES, Chaviaropoulos PK, Hansen AM, Madsen, H.A., Rasmussen, F., "Identification of structural non-linearities due to large deflections on a 5MW wind turbine blade," Proc. of EWEC'2008, Brussels, Belgium
- [9] Crisfield M. A., 1996, "Non-linear Finite Element Analysis of Solids and Structures Volume 1", Imperial College of Science
- [10] Voutsinas S. G., 2006, "Vortex methods in aeronautics: how to make things work", International Journal of Computational Fluid Dynamics, Vol. 20, pp. 3-18
- [11] Faltinsen O M, 1990, "Sea Loads on Ships and Offshore Structures", Cambridge University Press.
- [12] Cummins WE, 1962, "The Impulse Response Function and Ship Motions", Schiffstechnik, 9. Ocean Engineering, 13(6), pp. 505-538.